

Zero-Shot Video Semantic Segmentation based on Pre-Trained Diffusion Models

Qian Wang
KAUST
Saudi Arabia

Abdelrahman Eldesokey
KAUST
Saudi Arabia

Mohit Mendiratta
MPI for Informatics
Germany

Fangneng Zhan
MPI for Informatics
Germany

Adam Kortylewski
MPI for Informatics
Germany

Christian Theobalt
MPI for Informatics
Germany

Peter Wonka
KAUST
Saudi Arabia

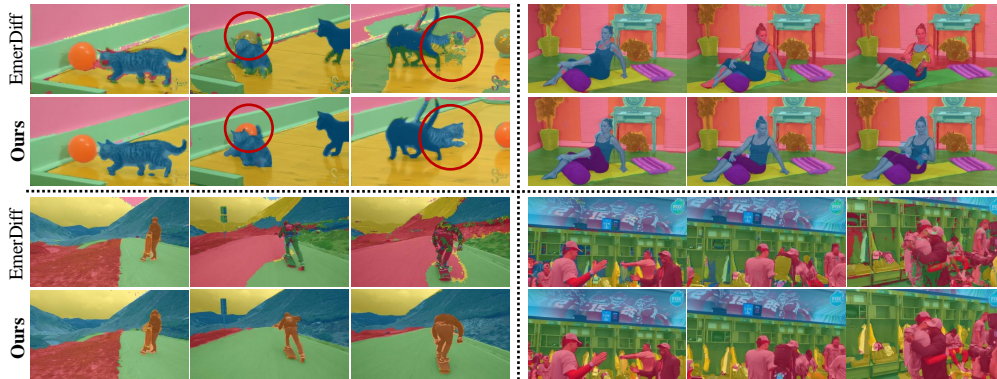


Figure 1: We propose the first *zero-shot* diffusion-based approach for Video Semantic Segmentation (VSS). Our approach produces temporally consistent predictions compared to the diffusion-based image segmentation method EmerDiff [14].

Abstract

We introduce the first *zero-shot* approach for Video Semantic Segmentation (VSS) based on pre-trained diffusion models. A growing research direction attempts to employ diffusion models to perform downstream vision tasks by exploiting their deep understanding of image semantics. Yet, the majority of these approaches have focused on image-related tasks like semantic correspondence and segmentation, with less emphasis on video tasks such as VSS. Ideally, diffusion-based image semantic segmentation approaches can be applied to videos in a frame-by-frame manner. However, we find their performance on videos to be subpar due to the absence of any modeling of temporal information inherent in the video data. To this end, we tackle this problem and introduce a framework tailored for VSS based on pre-trained image and video diffusion models. We propose building a scene context model based on the diffusion features, where the model is autoregressively updated to adapt to scene changes. This context model predicts per-frame coarse segmentation maps that are temporally consistent. To refine these maps further, we propose a correspondence-based refinement strategy that aggregates predictions temporally, resulting in more confident predictions. Finally, we introduce a masked modulation approach to upsample the coarse maps to the full resolution at a high quality. Experiments show that our proposed approach outperforms existing

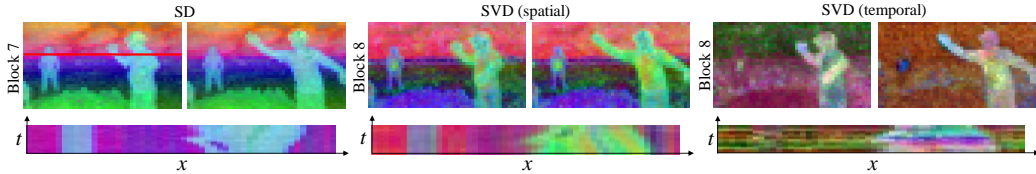


Figure 2: A visualization of the first three PCA components for the features of two video frames extracted from the most semantically-rich blocks in SD (Block 7) and SVD (Block 8). In the second row, we show the x - t slice of an image row (highlighted in the red line in the leftmost image) horizontally across the PCA visualization (x -axis) and stack it chronologically across the full batch of video frames (t -axis). The plot shows that the spatial features of both SD and SVD are temporally more consistent between video frames compared to the features of temporal layers in SVD.

zero-shot image semantic segmentation approaches significantly on various VSS benchmarks without any training or fine-tuning. Moreover, it rivals supervised VSS approaches on the VSPW dataset despite not being explicitly trained for VSS. We released our code in https://github.com/QianWangX/VidSeg_diffusion.

1 Introduction

Diffusion models [8, 18, 20, 16, 2] have showcased remarkable capabilities in learning real data distributions effectively, allowing them to generate high-quality images and videos with soaring diversity and fidelity. This was achieved by exploiting their scalability to train on large-scale datasets [1, 21]. Interestingly, those models were able to learn profound abstractions of images and their semantics as an indirect consequence of their large-scale training. This entitled them to be considered as *Foundation Models* that possess high degrees of generalizability and understanding of images. As a result, a growing direction of research attempts to use the internal representations of diffusion models to perform various downstream image vision tasks. For instance, pre-trained diffusion models were used to perform image semantic correspondence [22, 11], keypoints detection [7], and image semantic segmentation [14, 12].

Video vision tasks, on the other hand, have not received the same attention compared to their image counterparts. A simple approach is adopting image-based approaches to solve video tasks. For example, the diffusion-based image semantic segmentation approach EmerDiff [14] can be employed to perform Video Semantic Segmentation (VSS) in a frame-by-frame manner. However, our initial investigations show that it performs poorly in segmenting videos in terms of temporal consistency, as shown in Figure 1. This can be attributed to the lack of modeling of video temporal information, causing inconsistent predictions across frames.

An intuitive solution for enhancing the temporal consistency of these approaches is employing a video diffusion model, e.g., Stable Video Diffusion (SVD) [2] as a backbone. The SVD model is initially trained on images, then expanded with temporal layers and fine-tuned on videos. Ideally, the temporal features from SVD should exhibit better temporal consistency. To investigate this hypothesis, we visualize the temporal features of a pre-trained SVD in Figure 2 to examine their temporal consistency. The figure shows that the temporal features are surprisingly unstable and tend to change significantly between video frames. On the other hand, the spatial features encode the structure of the scene, similar to Image Stable Diffusion [19] (SD). Based on these observations, we capitalize on the spatial features of either SD or SVD and attempt to enhance them temporally.

In this paper, we introduce a diffusion-based zero-shot approach for VSS. First, we build a *scene context model* based on the features of a pre-trained image (SD) or video (SVD) diffusion model. This context model produces per-frame coarse segmentation maps and is autoregressively updated to accommodate scene changes throughout the video. To further enhance the temporal and spatial consistency of these coarse maps, we propose a correspondence-based refinement (CBR) strategy encompassing a pixel-wise voting scheme between the video frames. Finally, we propose a masked modulation process to reconstruct the full-resolution segmentation maps that is more stable and less noisy than that of [14]. Experiments show that our proposed approach significantly outperforms zero-shot image semantic segmentation methods on various VSS benchmarks. More specifically, we

improve mIOU over image semantic approaches by at least 29% on VSPW, CityScapes, and Camvid datasets. Remarkably, our approach performs comparably well as supervised VSS approaches on the diverse VSPW dataset. We also show that for currently released models, SD features lead to a higher quality result than SVD features, but this trend may reverse when SVD training considers larger datasets in the future.

2 Related Work

2.1 Diffusion Models’ Features

The large-scale training of diffusion models on the LAION-5B dataset [21] with 5 billion images allowed them to learn semantically rich image features. As a result, a growing direction of research attempts to employ these features to perform downstream vision tasks. Several approaches [11, 22, 25] investigated using these features to perform semantic correspondence. They observed that the features are semantically meaningful and generalize well across different objects and styles of images. For example, a human head in any arbitrary image will have similar features to any other human head in other images, regardless of the scene variations. Those features even generalize across similar classes of objects like animal heads. At the same time, the features will differ from those of unrelated object classes like buildings, landscapes, vehicles, *etc.* EmerDiff [14] capitalized on this observation to perform image semantic segmentation. Since the diffusion features are distinct for different objects, they can easily be clustered to separate those objects and produce a coarse segmentation map. Then, they proposed a modulation strategy to produce fine segmentation maps at a remarkable quality. However, we observed that the produced segmentation maps by EmerDiff are not temporally consistent, as illustrated in Figure 1, making it unsuitable for Video Semantic Segmentation (VSS). Therefore, we propose a diffusion-based pipeline tailored to improve the temporal consistency in VSS.

2.2 Video Semantic Segmentation

Video semantic segmentation (VSS) [23, 26, 27, 9, 28, 4, 24] is a spatiotemporal variation of image segmentation on videos that aims to predict a pixel-wise label across the video frames. Those predictions should be temporally consistent under object deformations and camera motion, making VSS more challenging than its image counterpart. Recent approaches attempted to exploit the temporal correlation between video features to produce temporally consistent predictions. Several approaches [29, 6] incorporated optical flow prediction to model motion between frames. Other approaches [10] proposed a temporal consistency loss on the per-frame segmentation predictions as an efficient replacement for optical flow. TMANet [23] utilized a temporal attention module to capture the relations between the current frame and a memory bank. DVIS [26] further improved the efficiency by treating VSS as a first-frame-segmentation followed by a tracking problem. Recent work UniVS [9] proposed a single unified model for all video segmentation tasks by considering the features from previous frames as visual prompts for the consecutive frames. Despite their remarkable performance, these supervised approaches do not generalize well on unseen datasets [27]. Therefore, it is desired to have an approach that generalizes well across datasets. Inspired by the success of EmerDiff [14] on image semantic segmentation, we attempt to exploit the diffusion features to propose the first temporally consistent zero-shot VSS approach.

3 Preliminaries

3.1 Stable Diffusion architecture

Stable Diffusion (SD) [19, 15] is one of the prominent latent diffusion models that achieves a good tradeoff between efficiency and quality. It is trained to approximate the real data distribution by adding noise to the latents of data samples until they reach pure Gaussian isotropic noise. During sampling, it performs a series of Markovian denoising steps starting from pure noise to recover a noise-free latent that is decoded to produce a synthetic image. SD utilizes a UNet architecture to predict either the noise or some other signal at each time step. This UNet encompasses multiple blocks for the encoder and the decoder at different resolutions ranging from 8×8 to 64×64 , where every

block has residual blocks, self-attention, and cross-attention modules. The attention is computed as:

$$f\left(\sigma\left(\frac{QK^T}{\sqrt{d}}\right)\cdot V\right) \quad (1)$$

where Q, K, V are the query, key, and value vectors in the attention layers, σ is the Softmax activation, and f denotes a fully connected layer. The query is always computed from the image features, while the key and the value are computed from the image in self-attention and a conditional signal (e.g. textual prompt) in cross-attention. Since the semantically rich features are located in the decoder [22, 14], We only consider the decoder blocks. The decoder has 12 blocks over 4 resolutions, where We refer to the first block as 0, with a resolution of 8×8 , and the last block as 11, with a resolution of 64×64 .

3.2 Emerging Image Semantic Segmentation from Diffusion Models

EmerDiff [14] observed that it is possible to extract semantically rich features from some of the UNet blocks and use them to produce coarse semantic segmentation maps. Given an RGB image X with a resolution of $H \times W$, the spatial resolution of the low-dimensional UNet features becomes $H/S_i \times W/S_i$, where S_i is the scale factor of block i determined by both the size of the latent representation and the downsampling factor of that block. By applying K-Means clustering on the low-dimensional feature maps from Block b_k at timestep t_k , we obtain a set of binary masks $\mathcal{M} = \{M_1, M_2, \dots, M_L\}$, where $M \in \mathbb{R}^{H/S_i \times W/S_i}$, and L is the number of distinct clusters.

A *modulation* strategy is used to obtain fine-grained image-resolution segmentation maps. This is achieved by modulating the attention module at block b_m and denoising timestep t_m for each binary mask M_l based on the following formula:

$$f\left(\sigma\left(\frac{QK^T}{\sqrt{d}}\right)\cdot V \pm \lambda M_l\right), \quad (2)$$

where λ controls the degree of modulation. The intuition behind this process is to add or subtract a certain amount of perturbation λ on the region specified by mask M_l and then continue the denoising process to reconstruct a modulated image. By applying $+\lambda$ and $-\lambda$, we get two different modulated images denoted as I_l^+ and I_l^- respectively. Then, a difference map is computed as $D_l = \|I_l^+ - I_l^-\|^2$, where $D_l \in \mathbb{R}^{H \times W}$. This is repeated for all masks in \mathcal{M} to get a set of difference maps $\mathcal{D} = \{D_1, D_2, \dots, D_L\}$. Finally, the full-resolution segmentation map is computed as $Y = \arg \max_l \mathcal{D}$.

4 Method

Our method encompasses three main components, as illustrated in Figure 3. First, we construct a *scene context model* to produce coarse segmentation maps based on the diffusion features (Section 4.1). Then, we introduce a *correspondence-based refinement* strategy to curate the coarse segmentation maps (Section 4.2). Finally, we propose a *masked modulation* approach that produces less noisy and more stable full-resolution segmentation maps (4.3). We also provide some details on adapting our approach to employ features from Stable Video Diffusion (SVD) in Section 4.4.

4.1 Scene Context Model

Image segmentation algorithms are designed for segmenting individual images and can only process videos in a frame-by-frame manner. This is not ideal for videos, as the per-frame predictions will be completely independent and consequently temporally inconsistent. To address this limitation, we propose to create a scene context model that is initialized at the first frame and then updated throughout the video in an autoregressive manner.

Given a video sequence $\mathcal{X} = \{X^1, X^2, \dots, X^N\}$ with N frames, we extract diffusion features F_i^n for all frames in $[1, N]$, where i is the decoder block. Since different blocks have different information, we aggregate features from multiple blocks by averaging to produce an aggregated feature \tilde{F}^n . We found that aggregating blocks 6, 7, and 8 attains the best results (see Section 5.4). Note that these blocks share the same resolution and number of channels. Then, we process the video in batches of length B .

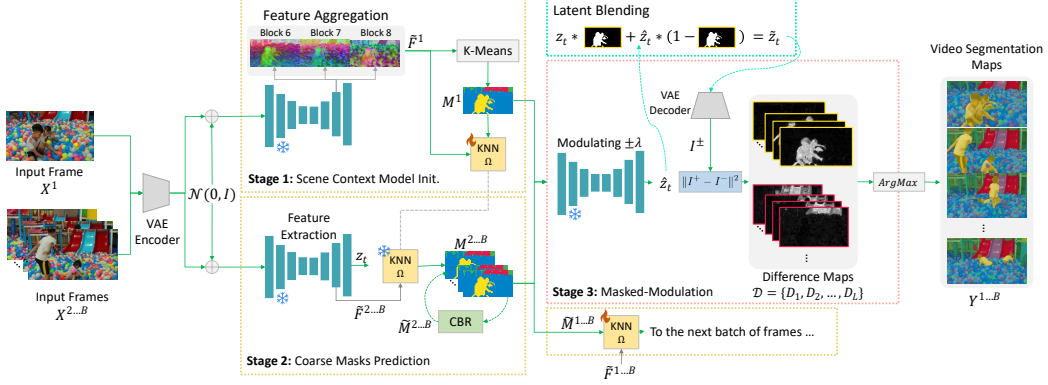


Figure 3: Our Video Semantic Segmentation (VSS) approach encompasses three stages. In Stage 1, we initialize a Scene Context Model Ω as a KNN classifier with the aggregated diffusion features \tilde{F}^1 of the first frame and a coarse mask M^1 produced by K-Means clustering. In Stage 2, we use the context model Ω to predict coarse masks for the remaining frames in the batch $M^{2...B}$. We refine the coarse maps $M^{1...B}$ using our correspondence-based refinement (CBR). In Stage 3, we use the refined coarse masks to modulate the attention layers of the diffusion process with factor $\pm\lambda$ to obtain a modulated latent \hat{z}_t . Then, we blend \hat{z}_t with the original unmodulated latent z_t using the coarse masks to obtain a less noisy latent \tilde{z}_t . Finally, the latent \tilde{z}_t is decoded to obtain images I^+, I^- that are used to compute a set of difference maps per segment $l \in L$. The final predictions are made by applying an arg max operation over the difference maps similar to [14]. The process is repeated for the following batch of frames where the context model is updated in an autoregressive manner using the coarse masks $M^{1...B}$ and their corresponding features $\tilde{F}^{1...B}$.

For the first batch, we use K-Means to extract the initial coarse segmentation map for the first frame M^1 based on the aggregated features \tilde{F}^1 . Given the diffusion features \tilde{F}^1 and the coarse map M^1 as labels, we train a KNN classifier $\Omega(M^1, \tilde{F}^1)$ as a context model to discriminate between different clusters. Then, we use the context model Ω to predict the coarse segmentation maps for the remaining frames in the first batch $\{M^2, M^3, \dots, M^B\}$. We refine the coarse maps further using the correspondence-based refinement (Section 4.2) and use them alongside their aggregated diffusion features to update the context model as $\Omega([\tilde{M}^1, \tilde{M}^2, \dots, \tilde{M}^B], [\tilde{F}^1, \tilde{F}^2, \dots, \tilde{F}^B])$. The context model is then used for the next batch. This strategy ensures that the context model Ω adapts to changes in the video in an auto-regressive manner.

4.2 Correspondence-Based Refinement

Since the context model operates purely in the feature space, it is unaware of the spatial arrangement of clusters or how they develop temporally. This might cause inconsistencies between clusters, especially across borders between objects. To alleviate this, we propose a refinement strategy based on the semantic correspondence between consecutive frames. We compute per-pixel correspondences (in the coarse map resolution) similar to [22] based on the diffusion features of block c between images j and $j + 1$ to produce a correspondence-based coarse segmentation \hat{M}^j :

$$\hat{M}^j[p] = \begin{cases} \arg \max_q \Gamma(F_c^j[p], F_c^{j+1}[q]), & \text{if } \|p - q\|^2 \leq \mathcal{T} \\ M^j[p], & \text{Otherwise} \end{cases}, \quad (3)$$

where Γ is a distance metric that we choose to be the cosine similarity. The threshold \mathcal{T} discards faulty matches that are spatially unfeasible. These correspondences are computed for all pixels p and over all frames within the batch. Finally, we perform a majority voting for all pixels over the temporal axis to produce the final coarse segmentation map \tilde{M}^j :

$$\tilde{M}^j[p] = \arg \max_{l \in L} \sum_{j=0}^{B-1} \mathbf{1}(\hat{M}^j[p] = l). \quad (4)$$

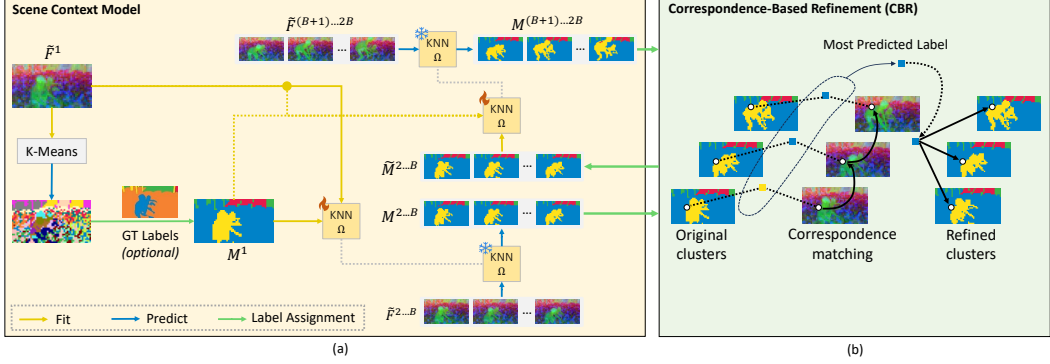


Figure 4: A detailed illustration of (a) the scene context model and (b) correspondence-based refinement.

Here, $\mathbf{1}(\hat{M}^j[p] = l)$ is an indicator function that equals 1 if $\hat{M}^j[p] = l$ and 0 otherwise. This interplay between the context model and the correspondence-based refinement leads to more accurate predictions. The context model encodes the feature space of the video batch, while the refinement strategy spatially and temporally regularizes the predictions. This setup is illustrated in Figure 4.

4.3 Masked Modulation

The modulation process aims to upsample the coarse segmentation masks to the full-resolution of the video frames. When applying the modulation process, it is only the modulated regions that are expected to change, as explained in Section 3.2. However, in practice, the modulation process produces noise outside that region, causing discrepancies when computing the final segmentation labels. Therefore, we propose a masked modulation process that employs the coarse segmentation map to mask out both the latents and the difference maps outside the modulated region. For a denoising timestep t , we blend the latents as follows:

$$\tilde{z}_t = z_t * (1 - M_l) + \hat{z}_t * M_l, \quad (5)$$

where z_t is the latent from the unmodified sampling step, \hat{z}_t is the latent from the modulated sampling process, and M_l is the low-resolution mask we are modulating. Despite the fact that the modulation is only performed at timestep t_m , we apply latent blending after t_m until timesteps t_f , as once the attention map of a certain timestep is modified, it will influence all the following denoising timesteps.

To further suppress the noise in the difference map, we can apply the same blending strategy to the difference maps. We compute the filtered difference map \tilde{D}_l as:

$$\tilde{D}_l = D_l * M_l + s \cdot D_l * (1 - M_l), \quad (6)$$

where s is a scaling hyperparameter that controls the filtering strength.

4.4 Adapting SVD for Video Semantic Segmentation

As it is natural to explore applying video models for video tasks, we further investigate the possibility of using Stable Video Diffusion (SVD)[2] features to perform VSS. Unlike SD, which is text-conditioned, SVD is image-conditioned. SVD adapts the SD 2.1 architecture and finetunes on a highly-curated large video dataset. Moreover, it employs a video VAE encoder to encode and decode the videos. SVD extends the SD architecture design mainly in two parts: 1) A video residual network that consists of a set of convolutional blocks that handle every frame of the video latent independently. 2) A temporal attention layer is applied on top of the output of the spatial attention layer, which computes the full attention of the features along the temporal axis on each spatial location. The output of the temporal attention and the output of the spatial attention are then mixed with a learnable weight. We use SVD as a backbone model to extract the features as well as do modulation following similar steps described in previous sections.

Table 1: Quantitative performance comparison.

Method	Backbone	Training	VSPW			Cityscapes	Camvid		
			mIoU	mVC ₈	mVC ₁₆	mIoU	mIoU	mVC ₈	mVC ₁₆
TMANet[23]	ResNet-50	Supervised	–	–	–	80.3	76.5	–	–
UniVS[9]	Swin-T	Supervised	59.8	92.3	–	–	–	–	–
DVIS++[26]	VIT-L	Supervised	63.8	95.7	95.1	–	–	–	–
CLIPpy	T5 + DINO	zero-shot	17.7	72.4	68.4	4.7	2.6	44.4	35.6
EmerDiff (SVD)	SVD	zero-shot	39.7	82.1	78.5	11.0	7.3	71.7	64.4
EmerDiff (SD)	SD 2.1	zero-shot	43.4	68.9	64.3	21.5	6.9	39.8	32.9
Ours(SVD)	SVD	zero-shot	53.2	89.3	88.0	36.2	16.6	87.4	85.8
Ours(SD)	SD 2.1	zero-shot	60.6	90.7	89.6	37.3	20.6	92.3	91.9

5 Experiments

To the best of our knowledge, no zero-shot diffusion-based Video Semantic Segmentation (VSS) approaches exist. Therefore, we compare against existing zero-shot image segmentation by adapting them to the VSS setting.

5.1 Experimental Setup

Implementation details. We evaluate our method with both SD 2.1 and SVD backbones, and we denote them as *Ours (SD)* and *Ours (SVD)*. Given the video frames, we encode them using VAE, and we add a certain level of noise that corresponds to timestep t_{inv} and start the denoising process at this noise level. As we need to perform modulation at timestep t_m , the value of t_{inv} must be larger than t_m . Initially, we set the modulating coefficient λ to 10 as in [14]. However, we observed that latent blending suppresses the modulating strength; thus, we increase λ to 50 when latent blending is enabled. We set the batch size $B = 14$, which is also the original training batch size of SVD.

We fix all hyperparameters for all videos and datasets, and we do not apply any post-processing methods like a conditional random field (CRF) on the output segmentation maps. All experiments were conducted on a single NVIDIA A100 40G GPU. We provide detailed parameter settings for SD and SVD backbones in Appendix.

Evaluation protocol. The clusters generated by K-Means in the first frame are class-agnostic. To be able to compare our predicted segmentation maps against the groundtruth, we use the labels from the groundtruth of the first frame to assign labels to our clusters. This is similar to the evaluation protocol in Video Object Segmentation, but we differ in that we only use the labels from the groundtruth and keep the segmentation masks from K-Means.

Baselines. We compare against zero-shot image segmentation approaches CLIPpy [17] and EmerDiff [14]. For EmerDiff, we adapt it to our zero-shot VSS setup. We use the same label assignment strategy for the first frame, but then we train a KNN classifier to predict the next frame in an autoregressive manner, similar to our approach. We also provide results of the supervised approaches DVIS++ [26], UniVS [9], and TMANet [23] to showcase where our zero-shot approach stands compared to them.

Dataset. We evaluate on the validation set of three commonly used VSS datasets: VSPW[13] with diverse videos, Cityscapes[5] and CamVid [3] with driving videos. VSPW has a resolution of 480p, while CamVid is 360p. For Cityscapes, to fit the video frames into GPU memory, we generate the segmentation maps at the resolution of 512×256 and upsample them to 2048×1024 for evaluation. We provide details of the settings for individual datasets in the Appendix.

Metrics. We report mean Intersection-over-Union (mIoU) and mean Video Consistency (mVC) [13] as quantitative metrics similar to existing VSS approaches [26, 27, 23]. mIoU describes the mean intersection-over-union between the predicted and ground truth pixels, while mVC computes the mean categories’ consistency over the long-range adjacent frames. We denote mVC evaluated under 8 and 16 video frames as mVC₈ and mVC₁₆, respectively. We use both metrics together to showcase the segmentation quality on individual images as well as the overall temporal consistency.



Figure 5: Qualitative comparison of different zero-shot methods. Note that the color of a segmentation cluster only represents the relative index of the clusters when the video is processed. The color itself does not map to an absolute label.

5.2 Quantitative results

We provide the quantitative results in Table 1. Our approach with both SD and SVD backbones performs the best in terms of all evaluation metrics on all datasets amongst the zero-shot approaches. More specifically, it improves over EmerDiff for both SD and SVD backbones in terms of mIoU with 33%, 29% on the VSPW dataset, 54%, 106% on the CityScapes dataset, and 99% and 78% on the Camvid dataset. Furthermore, our approach performs similarly to the supervised method UniVS and DVIS++ in terms of mIoU despite not being explicitly trained for this task. On the CityScapes and Camvid datasets, our approach outperforms the zero-shot methods by a huge margin. However, there is still a performance gap compared to the supervised approaches. We attribute this to two main reasons. First, CityScapes and Camvid datasets are for driving scenarios and have small objects and challenging lighting conditions, which poses a challenge when inverting the video frames (see Appendix). Secondly, we downsample their video frames of CityScapes by a factor of 16 to match the resolution of the diffusion models. This makes it difficult to segment small objects such as pedestrians and traffic poles, contrary to the VSS-specialized approaches that consider small objects when designing their solutions. We leave it for future work to adopt a tiled approach for high-resolution video segmentation.

5.3 Qualitative results

We show some qualitative results of different zero-shot methods in Figure 5. CLIPpy struggles to locate the boundaries accurately and produce coarse segments. EmerDiff can segment the first frame accurately but struggles to preserve the masks temporally. Our method with SD backbone produces the best segmentation maps in terms of segmentation quality and temporal consistency. The maps have sharper boundaries and clean clusters compared to other methods. Ours (SVD) performs better than its EmerDiff counterpart. However, the overall segmentation quality obtained by the SVD backbone is worse than that of SD. This can be attributed to the degraded feature representation of SVD compared to SD as a result of training on a relatively small video dataset compared to SD. We provide video results on our project website https://qianwangx.github.io/VidSeg_diffusion/.

5.4 Ablation Analysis

We show an ablation of our newly proposed components in Table 2. Incorporating more frames in training our context model greatly improves the mIoU as well as mVC. Enabling the masked modulation and the feature aggregation improves all metrics further. The best results in terms of mIoU are attained by enabling the correspondence-based refinement and disabling the feature aggregation. The feature aggregation can negatively impact the mIoU on some occasions due to the coarse groundtruth of the VSPW dataset. Figure 6 shows an example where our approach remarkably predicts the fine details of the window as one class and the background as another class, while

Table 2: Ablation study. The videos we use here are the first 30 videos from VSPW validation set. CBR refers to Correspondence-Based refinement.

Batch size B	Masked Modulation	Feature Aggregation	CBR	SD2.1			SVD		
				mIoU	mVC ₈	mVC ₁₆	mIoU	mVC ₈	mVC ₁₆
1	✗	✗	✗	33.4	70.6	60.2	26.6	82.2	78.3
14	✗	✗	✗	43.4	76.9	73.8	38.9	90.2	88.7
14	✓	✗	✗	45.6	87.5	85.5	38.6	90.5	89.0
14	✓	✓	✗	46.6	87.6	85.7	39.4	90.2	89.2
14	✓	✗	✓	47.4	89.2	87.5	37.1	91.5	90.3
14	✓	✓	✓	46.5	89.8	88.4	38.2	92.3	91.3

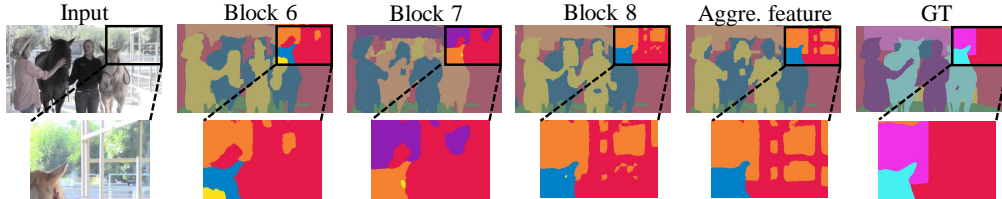


Figure 6: High-resolution segmentation map generated by aggregated feature has more details than features from a single block. We omit the low-resolution segmentation map for a better visual comparison.

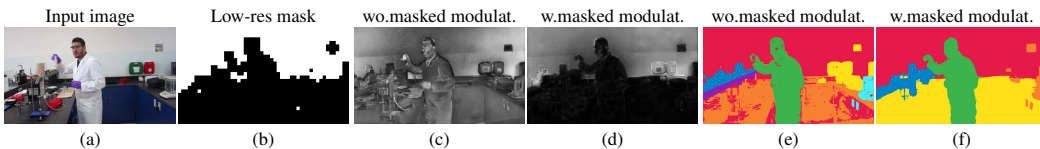


Figure 7: We show that given a low-resolution mask of a sub-region (b), the corresponding difference map without masked modulation (c) can have high activation outside the masked sub-region, which will result in spatial inconsistency on the final segmentation map (e). By applying masked modulation on the intermediate latents, the high activation on the irrelevant regions of the difference map will be removed (d), therefore producing a cleaner segmentation map (f).

the groundtruth annotates the whole region as a window. Finally, the best trade-off between the segmentation quality (mIoU) and temporal consistency (mVC) is achieved with all components.

Feature Aggregation. To validate the efficacy of feature aggregation, we show a visual comparison of the segmentation maps produced by features in different blocks in Figure 6. The aggregated features can encode more spatial details, which could enhance the coarse masks and, consequently, the high-resolution segmentation maps.

Masked Modulation. We show the qualitative comparison with or without the latent blending in Figure 7. The figure shows that without the latent blending, the difference map in (c) contains high activations outside of the modulated sub-region indicated by the coarse binary mask. The existence of activation in these regions can lead to a false assignment of the segmentation labels, as shown in (e). For example, a part of the lab table is classified as a wall. After applying latent blending, we remove activations outside of the mask region and obtain a cleaner segmentation mask, as shown in (f).

6 Limitations and Future Work

One of the limitations of our approach is its dependency on the quality of the image inversion method. Moreover, fine image details are likely to be discarded due to the compression from the VAE encoder. Therefore, our approach can benefit from future research improving both VAE encoding and image inversion. It is also beneficial to investigate if other video diffusion models have semantically higher quality features than SVD. Another limitation of our approach is that it is instance-agnostic, *i.e.* it groups all objects of the same class into the same cluster. This is due to the inherent nature of diffusion features that group similar semantics. For future work, our approach can be extended to perform Video Instance or Panoptic segmentation.

7 Conclusions

In this work, we introduced the first *zero-shot* method for Video Semantic Segmentation (VSS) using pre-trained diffusion models. We proposed a pipeline tailored for VSS that leverages image and video diffusion features, and attempts to enhance their temporal consistency. Experiments showed that our proposed approach significantly outperforms zero-shot image semantic segmentation methods on several VSS benchmarks, and performs comparably well to supervised methods on VSPW dataset.

References

- [1] Max Bain, Arsha Nagrani, Gül Varol, and Andrew Zisserman. Frozen in time: A joint video and image encoder for end-to-end retrieval. In *IEEE International Conference on Computer Vision*, 2021.
- [2] Andreas Blattmann, Tim Dockhorn, Sumith Kulal, Daniel Mendelevitch, Maciej Kilian, Dominik Lorenz, Yam Levi, Zion English, Vikram Voleti, Adam Letts, Varun Jampani, and Robin Rombach. Stable video diffusion: Scaling latent video diffusion models to large datasets, 2023.
- [3] Gabriel J. Brostow, Julien Fauqueur, and Roberto Cipolla. Semantic object classes in video: A high-definition ground truth database. *Pattern Recognition Letters*, 30(2):88–97, 2009. Video-based Object and Event Analysis.
- [4] Bowen Cheng, Anwesa Choudhuri, Ishan Misra, Alexander Kirillov, Rohit Girdhar, and Alexander G. Schwing. Mask2former for video instance segmentation, 2021.
- [5] Marius Cordts, Mohamed Omran, Sebastian Ramos, Timo Rehfeld, Markus Enzweiler, Rodrigo Benenson, Uwe Franke, Stefan Roth, and Bernt Schiele. The cityscapes dataset for semantic urban scene understanding. In *Proc. of the IEEE Conference on Computer Vision and Pattern Recognition (CVPR)*, 2016.
- [6] Raghudeep Gadde, Varun Jampani, and Peter V. Gehler. Semantic video cnns through representation warping, 2017.
- [7] Eric Hedlin, Gopal Sharma, Shweta Mahajan, Xingzhe He, Hossam Isack, Abhishek Kar Helge Rhodin, Andrea Tagliasacchi, and Kwang Moo Yi. Unsupervised keypoints from pretrained diffusion models. *arXiv preprint arXiv:2312.00065*, 2023.
- [8] Jonathan Ho, Ajay Jain, and Pieter Abbeel. Denoising diffusion probabilistic models. *Advances in neural information processing systems*, 33:6840–6851, 2020.
- [9] Minghan Li, Shuai Li, Xindong Zhang, and Lei Zhang. Univs: Unified and universal video segmentation with prompts as queries, 2024.
- [10] Yifan Liu, Chunhua Shen, Changqian Yu, and Jingdong Wang. Efficient semantic video segmentation with per-frame inference, 2020.
- [11] Grace Luo, Lisa Dunlap, Dong Huk Park, Aleksander Holynski, and Trevor Darrell. Diffusion hyperfeatures: Searching through time and space for semantic correspondence, 2023.
- [12] Pablo Marcos-Manchón, Roberto Alcover-Couso, Juan C. SanMiguel, and Jose M. Martínez. Open-vocabulary attention maps with token optimization for semantic segmentation in diffusion models, 2024.
- [13] Jiayu Miao, Yunchao Wei, Yu Wu, Chen Liang, Guangrui Li, and Yi Yang. Vspw: A large-scale dataset for video scene parsing in the wild. In *Proceedings of the IEEE/CVF Conference on Computer Vision and Pattern Recognition (CVPR)*, pages 4133–4143, June 2021.
- [14] Koichi Namekata, Amirmojtaba Sabour, Sanja Fidler, and Seung Wook Kim. Emerdiff: Emerging pixel-level semantic knowledge in diffusion models. In *The Twelfth International Conference on Learning Representations*, 2024.
- [15] Dustin Podell, Zion English, Kyle Lacey, Andreas Blattmann, Tim Dockhorn, Jonas Müller, Joe Penna, and Robin Rombach. Sdxl: Improving latent diffusion models for high-resolution image synthesis, 2023.
- [16] Aditya Ramesh, Prafulla Dhariwal, Alex Nichol, Casey Chu, and Mark Chen. Hierarchical text-conditional image generation with clip latents. *arXiv preprint arXiv:2204.06125*, 1(2):3, 2022.

- [17] K. Ranasinghe, B. McKinzie, S. Ravi, Y. Yang, A. Toshev, and J. Shlens. Perceptual grouping in contrastive vision-language models. In *2023 IEEE/CVF International Conference on Computer Vision (ICCV)*, pages 5548–5561, Los Alamitos, CA, USA, oct 2023. IEEE Computer Society.
- [18] Robin Rombach, Andreas Blattmann, Dominik Lorenz, Patrick Esser, and Björn Ommer. High-resolution image synthesis with latent diffusion models. In *Proceedings of the IEEE/CVF conference on computer vision and pattern recognition*, pages 10684–10695, 2022.
- [19] Robin Rombach, Andreas Blattmann, Dominik Lorenz, Patrick Esser, and Björn Ommer. High-resolution image synthesis with latent diffusion models, 2021.
- [20] Chitwan Saharia, William Chan, Saurabh Saxena, Lala Li, Jay Whang, Emily L Denton, Kamyar Ghasemipour, Raphael Gontijo Lopes, Burcu Karagol Ayan, Tim Salimans, et al. Photorealistic text-to-image diffusion models with deep language understanding. *Advances in Neural Information Processing Systems*, 35:36479–36494, 2022.
- [21] Christoph Schuhmann, Romain Beaumont, Richard Vencu, Cade Gordon, Ross Wightman, Mehdi Cherti, Theo Coombes, Aarush Katta, Clayton Mullis, Mitchell Wortsman, et al. Laion-5b: An open large-scale dataset for training next generation image-text models. *Advances in Neural Information Processing Systems*, 35:25278–25294, 2022.
- [22] Luming Tang, Menglin Jia, Qianqian Wang, Cheng Perng Phoo, and Bharath Hariharan. Emergent correspondence from image diffusion, 2023.
- [23] Hao Wang, Weining Wang, and Jing Liu. Temporal memory attention for video semantic segmentation. In *2021 IEEE International Conference on Image Processing (ICIP)*, pages 2254–2258. IEEE, 2021.
- [24] Shusheng Yang, Xinggang Wang, Yu Li, Yuxin Fang, Jiemin Fang, Liu, Xun Zhao, and Ying Shan. Temporally efficient vision transformer for video instance segmentation. In *Proc. IEEE Conf. Computer Vision and Pattern Recognition (CVPR)*, 2022.
- [25] Junyi Zhang, Charles Herrmann, Junhwa Hur, Luisa Polania Cabrera, Varun Jampani, Deqing Sun, and Ming-Hsuan Yang. A tale of two features: Stable diffusion complements dino for zero-shot semantic correspondence. *Advances in Neural Information Processing Systems*, 36, 2024.
- [26] Tao Zhang, Xingye Tian, Yu Wu, Shunping Ji, Xuebo Wang, Yuan Zhang, and Pengfei Wan. Dvis: Decoupled video instance segmentation framework, 2023.
- [27] Tao Zhang, Xingye Tian, Yikang Zhou, Shunping Ji, Xuebo Wang, Xin Tao, Yuan Zhang, Pengfei Wan, Zhongyuan Wang, and Yu Wu. Dvis++: Improved decoupled framework for universal video segmentation, 2023.
- [28] H. Zhao, J. Shi, X. Qi, X. Wang, and J. Jia. Pyramid scene parsing network. In *2017 IEEE Conference on Computer Vision and Pattern Recognition (CVPR)*, pages 6230–6239, 2017.
- [29] Xizhou Zhu, Yuwen Xiong, Jifeng Dai, Lu Yuan, and Yichen Wei. Deep feature flow for video recognition, 2017.

A supplemental material

A.1 Codebase and website

Our anonymized code is available at https://anonymous.4open.science/r/VidSeg_Anonymous-827E. We also provide video results on the anonymous project page https://anonymous.4open.science/w/VidSeg_Anonymous-E341-website/.

A.2 Broader impact

Video semantic segmentation has important applications in autonomous driving and surveillance security. However, the source videos used for segmentation may contain private information such as human faces and driving plates. Guidelines for responsible usage need to be made to prevent privacy invasion. Also, diffusion models can inherit and propagate biases from their training data, leading to unfair treatment of certain groups.

A.3 Settings

Dataset. VSPW (Video Scene Parsing in the Wild) is a large-scale video semantic segmentation dataset that consists of a wide range of real-world scenarios and categories. It has 124 categories in total. The resolution of this dataset is 480×853 . Since each video consists of less than 10 classes, we set the number of clusters for KMeans as 20. Cityscapes is a large-scale urban streets video sequence dataset. The objects are grouped into 30 classes in total. Each video clip has 30 frames, and only the 20th frame has dense annotations. We use its validation set, which contains 15000 frames from three cities. As the original resolution of the frames is 1024×2048 , which is too big to fit into the GPU memory with SVD, we downsample the frames to 256×512 for all the experiments and evaluate at the original resolution by upsampling the segmentation maps. As each video clip may contain classes of more than 10, we set the number of clusters as 30 in order to capture the small objects. CamVid (Cambridge-driving Labeled Video Database) is a road scene dataset with dense segmentation annotations with 11 classes in total. The resolution of this dataset is 360×480 . We use its validation set, which has one video clip and contains 100 frames. We set the number of clusters for KMeans as 20.

Implementation details. We build our method on top of SD 2.1 and SVD code repository <https://github.com/Stability-AI/generative-models>.

Computational resources. We use one NVIDIA A100 GPU to conduct all our experiments. As the running time depends on the number of clusters and spatial resolution of the video frames, generally, it will take around 2 minutes to process a batch of video frames using SD 2.1 and 5 minutes using SVD. The main cost of the time comes from the modulating process, which involves several modified forward passes of the backbone model.

A.4 Hyperparameters

We provide all hyperparameters for SD 2.1 and SVD in Table 3.

A.5 Failure cases

We identify several typical failure cases in our method. The first one is the inaccurate diffusion inversion process (Figure 8). In adjacent frames, the texture and shape details of the small objects can be different after inversion. Segmentation maps will also inherit this discrepancy between input frames and reconstructed frames, which will result in flickering on the frames. The second one is flickering between similar regions (Figure 9). Some objects are originally assigned with one cluster, while in the later frames, they are grouped into different clusters. The third one is dealing with unseen objects (Fig. 10). As we only use an anchor frame’s ground truth to guide the class-agnostic clusterings, we cannot handle well the unseen objects in the anchor frame.

Table 3: Hyperparameters settings for SD and SVD.

	Ours (SD 2.1)	Ours (SVD)
t_f	25	25
t_m	20	17
Sampling timesteps	25	25
Sampler	EDM	EDM
Block b_k	Block 6, 7 and 8	Block 6, 7 and 8
Block b_m	Block 7	Block 8
Block c	Block 7	Block 8
Spatial threshold \mathcal{T}	1	1
Filtering strength s	0.7	0.7
Modulating factor λ	50.0	50.0
Modulating attention type	cross attention	self attention
Injected features	spatial attention	spatial & temporal attention



Figure 8: Failure case: inversion. In adjacent frames, the car and the sign of the car experience shape changes, which finally result in obvious shape changes on the segmentation maps. We highlight the main areas of discrepancy in green and blue circles.

A.6 Ablation study

We provide additional ablation experiments here. We ablate the modulating Block b_m in Figure 11 for both SD and SVD. Modulating Block 7 and Block 8 for SD and SVD, respectively, can give the most spatial details as well as maintain the semantics. These blocks are, at the same time, the most semantically-riched blocks in SD and SVD. In Figure 12, we show more examples of how latent blending and difference map filtering help with removing spatial noises. In Figure 13, we show comparisons between the difference maps and segmentation maps produced by SD and SVD. We show that the difference maps of SD contain finer details, which bring sharper boundaries to the final segmentation maps. We further show PCA visualization of a 64×64 resolution block to complement Figure 2 in the main paper. We show that in high-resolution blocks, SD features have more semantic information and spatial details, as well as more temporally stable than SVD spatial features and temporal features. We also show that segmentation maps under different numbers of K-Means clusters and after GT labels reassignment in Figure 14. Increasing the number of clusters can help segment more small objects (from 5 to 20). However, further increasing the number of clusters may not necessarily segment out the clusters that are aligned with defined clusters in ground truth (from 20 to 30). Although K-Means originally generated 30 clusters, most of them are merged to the same classes after GT label reassignment.

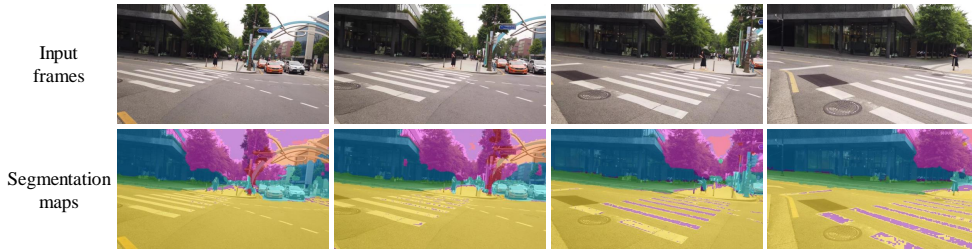


Figure 9: Failure case: temporal inconsistency. The sidewalk is clustered into the yellow region in the first frame, and later the same sidewalk is clustered into another region denoted as purple region.

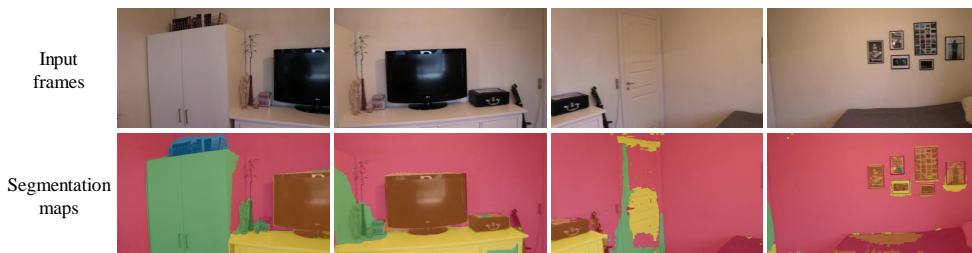


Figure 10: Failure case: unseen objects. The door and albums, which do not appear in the previous frames, are assigned with the wrong clusters.

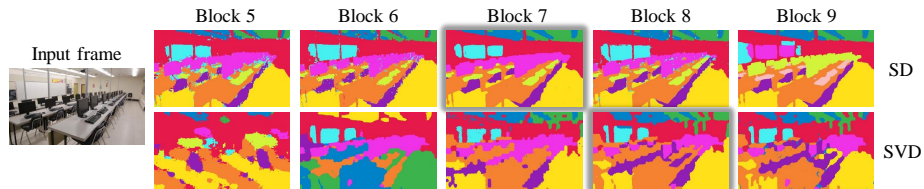


Figure 11: Ablation: modulating different block will result in different segmentation maps. Modulating Block 7 and Block 8 give the best results for SD and SVD, respectively (highlighted in shadow).

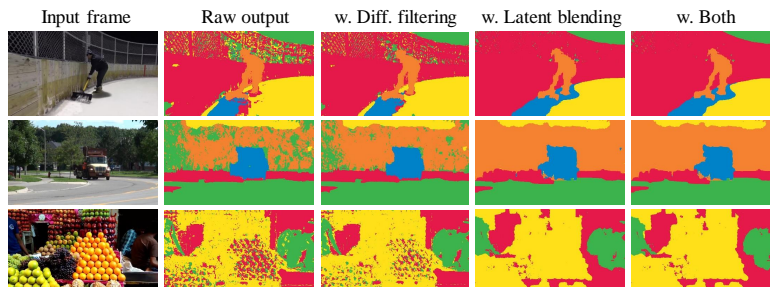


Figure 12: Ablation: latent blending and difference map filtering.

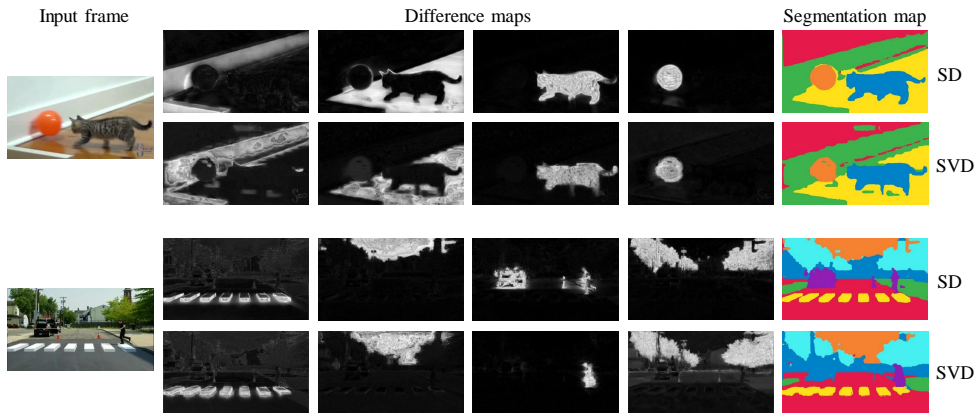


Figure 13: Ablation: Difference maps comparison between SD and SVD.

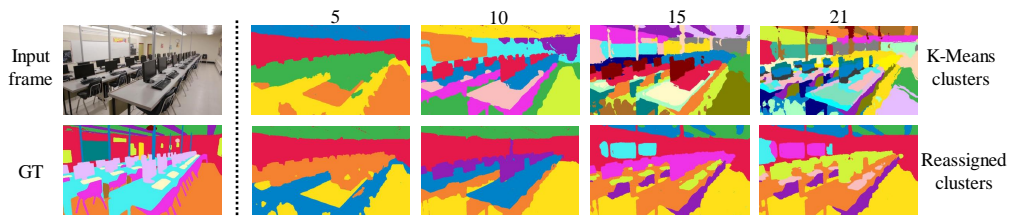


Figure 14: Ablation: number of K-Means clusters. In the first row, we show the segmentation maps generated by different numbers of clusters in K-Means. In the second row, we show the segmentation maps generated by the same numbers of clusters followed by GT labels reassignment.

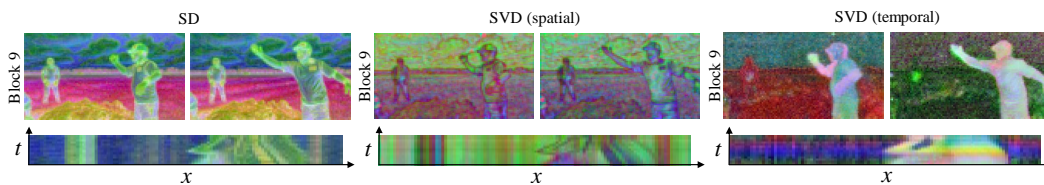


Figure 15: A visualization of the first three PCA components for the features extracted from the most semantically-rich blocks of Block 9 in both SD and SVD of the first and last video frames in a batch. In the second row, we show the $x-t$ slice of a set of pixels (highlighted in the red line in the leftmost PCA visualization) horizontally across the PCA visualization (x -axis) and stack it chronologically across the full batch of video frames (t -axis).